Available online at www.sciencedirect.com
ScienceDirect
International Journal of Heat and Fluid Flow 28 (2007) 1013–1026
International Journal of HEAT AND FLUID FLOW
www.elsevier.com/locate/ijhff

Performance analysis of nanofluid-cooled microchannel heat sinks

Tsung-Hsun Tsai [a], Reiyu Chein [b,*]

[a] Department of Mechanical Engineering, Wufeng Institute of Technology, Chia-Yi 621, Taiwan
[b] Department of Mechanical Engineering, National Chung Hsing University, 250 Kuo-Kuang Road, Taichung 402, Taiwan

Received 23 July 2006; received in revised form 14 November 2006; accepted 30 January 2007
Available online 23 March 2007

Abstract

Microchannel heat sink (MCHS) performance using copper–water (Cu–H_2O) and carbon nanotube–water (CNT–H_2O) nanofluids as coolants is addressed analytically in this study. The velocity and temperature distributions in the MCHS were obtained by modeling the MCHS as a porous media. The resulting velocity and temperature were then used to evaluate the thermal resistance that characterizes MCHS performance. It was found that the nanofluid reduced the temperature difference between the MCHS bottom wall and bulk nanofluid compared with that from pure fluid. This temperature difference produces a reduction in conductive thermal resistance, which is one of the two sources contributing the total thermal resistance of the MCHS. The other source of thermal resistance, termed as convective thermal resistance, was found to increase when nanofluid is employed as the coolant due to the increase in viscosity and decrease in thermal capacity. Under the condition of a given pressure drop across the MCHS, optimum values of aspect ratio and porosity that producing the minimum thermal resistance can be found. It was found that using nanofluid can enhance the MCHS performance when the porosity and aspect ratio are less than the optimum porosity and aspect ratio. When the porosity and channel aspect ratio are higher than optimum porosity and aspect ratio, the nanofluid did not produce a significant change in MCHS thermal resistance.

Keywords: Microchannel heat sink (MCHS); Nanofluid, Aspect ratio; Porosity; Convective thermal resistance and conductive resistance

1. Introduction

With the advances in computing technology over the past few decades, electronics have become faster, smaller and more powerful. This results in an ever-increasing heat generation rate from electronic devices. In most cases, the chips are cooled using forced air flow. However, when dealing with a component that contains billions of transistors working at high frequency, the temperature can reach a critical level where standard cooling methods are not sufficient. In addition to high-performance electronic chips, high heat flux removal is also required in devices such as laser diode arrays and high-energy mirrors. In the last two decades, many cooling technologies have been pursued to meet the high heat dissipation rate requirements and maintain a low junction temperature. Among these efforts, the microchannel heat sink (MCHS) has received much attention because of its ability to produce high heat transfer coefficient, small size and volume per heat load, and small coolant requirements. Recent progress in MCHS development was provided by Kandlikar et al. (2003).

A MCHS typically contains a large number of parallel microchannels with a hydraulic diameter ranging from 10 to 1000 μm. A coolant is forced to pass through these channels to carry the heat away from a hot surface. The MCHS cooling concept was proposed by Tuckerman and Pease (1981). Since then, MCHS performances with different substrate materials and channel dimensions have been studied extensively in the past two decades. These studies can be categorized into theoretical (Knight et al., 1992; Ambatipudi and Rahman, 2000), numerical (Fedorov and Viskanta, 2000; Lee et al., 2005; Li et al., 2004; Li and Peterson, 2006), and experimental approaches (Qu and Mudawar, 2002; Tiselj et al., 2004). In the theoretical approach, the main objective is to develop design schemes

* Corresponding author. Tel.: +886 4 22850462; fax: +886 4 22877170.
E-mail address: rychein@dragon.nchu.edu.tw (R. Chein).

0142-727X/$ - see front matter © 2007 Elsevier Inc. All rights reserved.
doi:10.1016/j.ijheatfluidflow.2007.01.007

Nomenclature

A_{eff}	effective heat transfer area, m^2
a	wetted area per volume of porous media, m^{-1}
Bi	Biot number
c_p	specific heat, $J\,kg^{-1}\,K^{-1}$
Da	Darcy parameter
H	depth of the microchannel, m
h	interfacial heat transfer coefficient between solid and fluid phase phases, $W\,m^{-2}\,K^{-1}$
$\bar{h}$	overall heat transfer coefficient of microchannel heat sink, $W\,m^{-2}\,K^{-1}$
K	permeability
k_{fe}	effective fluid phase conductivity, $W\,m^{-2}\,K^{-1}$
k_{se}	effective solid phase conductivity, $W\,m^{-2}\,K^{-1}$
k_d	thermal dispersion conductivity, $W\,m^{-2}\,K^{-1}$
L_{hs}	heat sink length, m
N	number of microchannels
P	dimensionless pressure drop
p	volume-averaged pressure, $N\,m^{-2}$
Pow	pumping power, W
q_w	heat flux, $W\,m^{-2}$
u	volume-averaged fluid velocity, $m\,s^{-1}$
u_m	mean velocity in channel, $m\,s^{-1}$
R_{th}	heat sink total thermal resistance, °C W^{-1}
R_{flow}	heat sink convective thermal resistance, °C W^{-1}
R_{fin}	heat sink conductive thermal resistance, °C W^{-1}
SH	particle shape factor
T	temperature, K
T_b	bulk fluid temperature, K
T_w	wall temperature, K
$\dot{V}$	coolant volumetric flow rate, mL/min
W_{ch}	width of microchannel, m
W_{fin}	width of microchannel wall (fin), m
W_{hs}	heat sink width, m

Greek symbols

α_s	aspect ratio
ε	porosity
μ	viscosity, $kg\,m^{-1}\,s^{-1}$
ρ	density, $kg\,m^{-3}$
ϕ	particle volume fraction, %
ψ	sphericity
θ	dimensionless temperature

Subscripts

f	pure fluid
nf	nanofluid
p	particle
s	solid phase

that can be used to optimize MCHS performance. Most studies in this approach employed the classical fin theory which models the solid walls separating microchannels as thin fins. The heat transfer process is simplified as one-dimensional, constant convection heat transfer coefficient and uniform fluid temperature. However, the nature of the heat transfer process in MCHS is conjugated heat conduction in the solid wall and convection to the cooling fluid. The simplifications used in the theoretical approach usually under- or over predict MCHS performance.

To overcome the shortcomings associated with MCHS thermal performance analysis using fin theory, several investigators proposed modeling the MCHS as a porous medium. In the study by Kim and Kim (1999), laminar heat transfer in MCHS was analyzed using a modified Darcy model for fluid flow and two-equation model for heat transfer. They found that their results agreed well with those predicted using fin theory models (Knight et al., 1992) and experimental measurements by Tuckerman and Pease (1981). Zhao and Lu (2002) further extended the model developed by Kim and Kim (1999) to study the channel geometries, effective thermal conductivities and porosities on MCHS thermal performance. Because conjugated heat transfer is involved in MCHS, it is believed that the porous medium model is better than the classical fin theory in describing MCHS thermal performance.

Although high thermal performance can be achieved using MCHS, further improvement is still needed to cope with the increasing demands from various device applications. From the heat transfer point of view, improving MCHS thermal performance enhances the heat transfer characteristics inside the MCHS. Extensive reviews on the techniques for heat transfer enhancement in macro-scale dimensions were provided by Bergles (2002) and Webb (1993). One of the methods for enhancing heat transfer is the application of additives to the working fluids. The basic idea is to enhance the heat transfer by changing the fluid transport properties and flow features. In earlier studies, metal particles embedded in the liquid fluid were used to enhance the heat exchanger performance. However, a serious clogging problem occurred due to the particle sedimentation. Recent interest based on this concept focused on heat transfer enhancement using a nanofluid in which nanoscale metallic or non-metallic particles were suspended in the base fluids. Several experimental and analytical studies showed that nanofluids have higher thermal conductivity than pure fluids and therefore greater potential for heat transfer enhancement (Wang et al., 1999; Koo and Kleinstreuer, 2004).

Using a nanofluid as the heat transfer working fluid has gained much attention in recent years. Xuan and Roetzel (2000) proposed two theoretical models to predict the heat transfer characteristics of nanofluid flow in a tube. Li and Xuan (2002), Xuan and Li (2003) and Pak and Cho (1998) experimentally measured the convection heat transfer and pressure drop for nanofluid tube flows. Their results

indicated that the heat transfer coefficient was greatly enhanced and depended on the flow Reynolds number, particle Peclet number, particle size and shape, and particle volume fraction. These studies also indicated that the presence of nanoparticles did not cause an extra pressure drop in the flow. Recently, Yang et al. (2005) carried out an experimental study attempting to construct a heat transfer correlation among the parameters that affected heat transfer. For a laminar flow regime in a circular tube, they indicated that the heat transfer coefficient for the nanofluid flow had a lower increase than predicted by either the conventional heat transfer correlation for the homogeneous or particle-suspended fluid. Ding et al. (2006) reported heat transfer coefficient data for the force convection in circular tubes using carbontube (CNT) nanofluid.

In most of the studies mentioned above, the nanofluid heat transfer flow characteristics were carried out in macro-scale dimensions. Only a few studies addressed the nanofluid flow and heat transfer in micro-scale dimensions. In numerical aspect, Koo and Kleinstreuer (2005) and Jang and Choi (2006) studied the MCHS performance numerically using different models for the effective thermal conductivity of the nanofluids. Chein and Hunag (2005) employed a macro-scale correlation to predict microchannel heat sink performance. In experimental aspect, Chein and Chuang (2007) studied the general behavior heat sink performance and particle deposition effect when nanofluid is used as the working fluid. In the study of Lee and Mudawar (2006), Al_2O_3–H_2O nanofluid was used as working fluid. They pointed out that the high thermal conductivity of nanoparticles can enhance the single-phase heat transfer coefficient, especially for the laminar flow. Due to complicated heat transfer phenomena and large variety in nanofluids, further studies on nanofluid flow and heat transfer characteristics in micro-scale dimensions are still necessary. In this study, thermal resistance characterizing MCHS performance using nanofluids as coolants are investigated. We particularly focus on the microchannel geometry effect on the MCHS performance when nanofluid is used as the working fluid. The MCHS is modeled as a porous media. Fluid velocity and temperature distribution details in a MCHS and their relations with the sources that contribute to thermal resistance during MCHS cooling will be discussed.

2. Mathematical model

2.1. Assumptions

In this study, the nanofluid is to be used as the working fluid in the MCHS operation. Fundamentally, nanofluid is a mixture of solid particles and base fluid. The difference between nanofluid and the traditional solid/fluid mixture is the particle size. In the traditional solid/liquid mixture, the typical particle size is of the order of μm while particle size of order of nm is involved in the nanofluid. When the traditional two-phase mixture used as a working fluid in flow system, local non-equilibrium between the particle and fluid, i.e., velocity slip and temperature difference between particle and fluid, are taken into account in the governing equations for both particle and fluid phases. In the past, governing equations for two-phase flow system have been well established (Crowe et al., 1998). Unlike the traditional two-phase mixture, nanofluid has ultra-fine particles suspended in the base fluid. Several factors such as thermal dispersion, intermolecular energy exchange, liquid layering on the solid–liquid interface, and photon effects on the heat transport inside the particles may affect the fluid flow and heat transfer when nanofluid is employed as the working fluid. Moreover, the local thermally non-equilibrium between the base fluid and nanoparticle may also exist due to the large difference in thermal conductivities. To our best knowledge, governing equations including these complicated phenomena are still under development (Maiga et al., 2005). Because of this difficulty, the alternative way to investigate the fluid flow and heat transfer is based on treating the nanofluid as a single-phase fluid. As pointed out by Xuan and Roetzel (2000), this assumption may be applicable since the particles are ultrafine and they are easily fluidized. Moreover, the particle volume fraction in nanofluid is usually low. Under such assumption, the governing equations for the nanofluid flow and heat transfer are greatly simplified and local fluid and particles are in thermal equilibrium.

2.2. Governing equations

Fig. 1 shows the geometric configuration of MCHS under consideration. The opened microchannels have a width of W_{ch} and depth of H, were fabricated on a silicon wafer substrate. The top side of the fabricated microchannels is bonded with a glass cover plate to form closed microchannels. After bonding, the substrate is cut to form the MCHS with width W_{hs}, length L_{hs} and a base plate thickness of t_b. The walls that separate the channels are called fins with a width of W_{fin}. The MCHS top wall is assumed insulated while the bottom wall receives a uniform

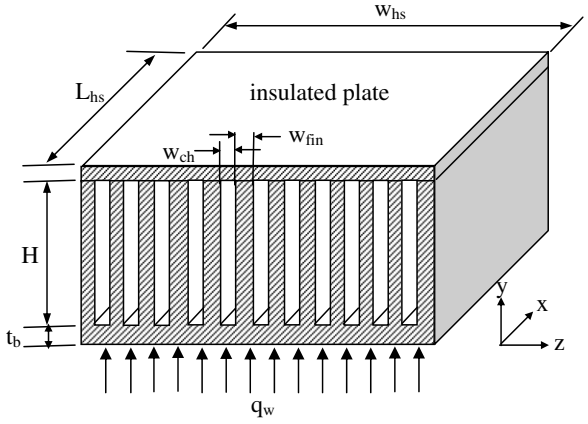

Fig. 1. Schematic diagram of the microchannel heat sink.

heat flux q_w. The heat flux can be thought of as the heat needed to be dissipated from a cooled object such as an electronic chip or laser diode array. The coolant, a pure fluid or nanofluid, is forced through the channels in the x-direction to achieve the heat dissipation.

As proposed by Kim and Kim (1999), the MCHS can be modeled as a porous micro-structure. That is, the region between the cover plate and base plate of the MCHS is modeled as a porous medium. The governing equations for the fluid flow and heat transfer can be established by applying the volume-averaged technique. Since the one-equation model is valid only when the fluid phase is in local equilibrium with the solid phase and is not suitable in the evaluation of MCHS thermal performance (Kim et al., 2000), the two-equation model is employed in this study. Under the assumption of treating nanofluid as single-phase fluid, the governing equations for the fluid and energy transport under fully hydrodynamic and thermal development conditions can be written as

Fluid flow:

$$-\frac{dp}{dx}+\mu_f\frac{d^2u}{dy^2}-\frac{\mu_f}{K}\varepsilon u=0 \tag{1}$$

Energy in solid phase:

$$k_{se}\frac{\partial^2 T_s}{\partial y^2}=ha(T_s-T_f) \tag{2}$$

Energy in fluid phase:

$$\varepsilon(\rho c_p)_f u\frac{\partial T_f}{\partial x}=ha(T_s-T_f)+\frac{\partial}{\partial y}\left(k_{fe}\frac{\partial T_f}{\partial y}\right) \tag{3}$$

In Eqs. (1)–(3), p, u, T_f, T_s and h are the volume-averaged fluid pressure, fluid velocity, fluid temperature, solid temperature and interfacial heat transfer coefficient between fluid and solid, respectively. The MCHS shown in Fig. 1, modeled as a porous medium, the porosity ε, permeability K and wetted area per volume a can be expressed as (Bejan, 1984)

$$\varepsilon=\frac{W_{ch}}{W_{ch}+W_{fin}},\quad K=\frac{\varepsilon W_{ch}^2}{12},\quad a=\frac{2(W_{ch}+H)}{(W_{ch}+W_{fin})H} \tag{4}$$

As appeared in Eqs. (1)–(3), the thermophysical properties of fluid and solid involved are the fluid density ρ_f, fluid viscosity μ_f, fluid thermal capacity $(\rho c_p)_f$, fluid effective thermal conductivity k_{fe} and solid effective conductivity k_{se}. The effective thermal conductivities of the fluid and solid phases can be written as (Bejan, 1984)

$$k_{se}=(1-\varepsilon)k_s,\quad k_{fe}=\varepsilon k_f \tag{5}$$

Based on the thermally fully developed flow, the energy balance between the fluid flow and applied heat flux can be related as

$$q_w=\varepsilon(\rho c_p)_f u_m H\frac{\partial T_f}{\partial x} \tag{6}$$

where u_m is the mean fluid velocity. Substituting Eq. (6) into Eq. (3), the energy equation for the fluid flow can be written as

$$\frac{u}{u_m}\frac{q_w}{H}=ha(T_s-T_f)+\frac{\partial}{\partial y}\left(k_{fe}\frac{\partial T_f}{\partial y}\right) \tag{7}$$

To complete the mathematical model, the boundary conditions are needed. Based on the physical model depicted in Fig. 1, the boundary conditions for Eqs. (1), (2) and (7) are

$$\text{At } y=0: \quad u=0,\quad T_s=T_f=T_w \tag{8a}$$

$$\text{At } y=H: \quad u=0,\quad \frac{\partial T_s}{\partial y}=\frac{\partial T_f}{\partial y}=0 \tag{8b}$$

In writing Eq. (8a), we have neglected the influence of the MCHS base plate thickness since the MCHS material usually has high thermal conductivity. The temperature T_w is regarded as the temperature of the MCHS bottom wall.

As shown in Eq. (7), the interfacial heat transfer coefficient is also one of the important parameters in dealing with the heat transfer in porous media. Since the porous medium originates from the rectangular channels, the interfacial heat transfer coefficient in a rectangular channel flow can be used. A well-established relation for the heat transfer coefficient for the rectangular channel flow under thermally fully development is given as (Knight et al., 1992)

$$h=\frac{k_f}{D_h}\left[-1.047+9.326\frac{\alpha_s^2+1}{(\alpha_s+1)^2}\right] \tag{9}$$

where α_s and D_h are the aspect ratio and hydraulic diameter of the channel defined as

$$\alpha_s=\frac{H}{W_{ch}},\quad D_h=\frac{2HW_{ch}}{W_{ch}+H} \tag{10}$$

2.3. Thermophysical properties of nanofluid

In this study, the nanofluid is to be used as the working fluid. The thermophysical properties involved in the governing equations are replaced by those of the nanofluid. That is, ρ_f, $(\rho c_p)_f$, k_f and μ_f are to be replaced by ρ_{nf}, $(\rho c_p)_{nf}$, k_{nf} and μ_{nf}, respectively. These properties are given as

$$\text{Density}: \quad \rho_{nf}=(1-\phi)\rho_f+\phi\rho_p \tag{11}$$

$$\text{Thermal capacity}: \quad (\rho c_p)_{nf}=(1-\phi)(\rho c_p)_f+\phi(\rho c_p)_p \tag{12}$$

$$\text{Thermal conductivity}: \quad k_{nf}=k_0+k_d \tag{13a}$$

$$k_0=k_f\frac{k_p+(SH-1)k_f-(SH-1)\phi(k_f-k_p)}{k_p+(SH-1)k_f+\phi(k_f-k_p)} \tag{13b}$$

$$\text{Viscosity}: \quad \mu_{nf}=\mu_f\frac{1}{(1-\phi)^{2.5}} \tag{14}$$

As shown in Eqs. (11)–(14), thermophysical properties of nanofluid is related to the particle volume fraction which is defined as the fraction of volume occupied by particle in a unit volume of bulk fluid. The density and thermal

capacity of nanofluid are simply evaluated based on the volume fractions of each phase composed of nanofluid as shown in Eqs. (11) and (12). In recent years, there have been many researches devoting into evaluating the thermal conductivity of nanofluid (Wang et al., 1999; Lee et al., 1999). Because the nanofluid can be made using large varieties of nanoparticles, base fluid and particle volume fractions, the results from these studies show a large variety in nanofluid thermal conductivity. Fundamentally, the thermal conductivity of nanofluid is related to the particle volume fraction of each phase, particle shape and thermal dispersion due to the chaotic motion of nanoparticles in the bulk flow. The thermal conductivity of nanofluid as shown in Eq. (13a) composes of two terms to account for these effects. The first term k_0 is regarded as the theoretical model for the nanofluid thermal conductivity proposed by Hamilton and Crosser (1962) based on treating nanofluids as liquid–solid mixtures under static conditions. In addition to the thermal conductivities of the particle and fluid, the thermal conductivity of the nanofluid under static conditions also depends on the shape factor of the nanoparticle which is given as

$$\mathrm{SH} = \frac{3}{\psi} \tag{15}$$

where ψ is the sphericity defined as the ratio of the surface area of a sphere with a volume equal to that of the particle to the surface area of the particle. Although recent studies indicated that Eq. (13b) underestimates the thermal conductivity of the nanofluid (Wang et al., 1999; Koo and Kleinstreuer, 2004; Wang and Mujumdar, 2007), it is usually employed as a comparison basis since fundamental factors that affecting the nanofluid thermal conductivity are included.

Although the assumption of treating nanofluid as a single-phase fluid greatly simplifies the fluid flow heat transfer analysis, the thermal dispersion effect due to nanoparticle random motion should not be neglected since it is one of the factors for heat transfer enhancement by using the nanofluid. The most direct way to establish a model for the thermal dispersion would be performing the experiments. By comparing the experimental measured heat transfer coefficient data for both pure fluid and nanofluid, the model for the thermal dispersion could be established. Although many experimental studies on convective heat transfer using nanofluid have been performed in the past, to our best knowledge, no conclusive correlation for the thermal dispersion is available at the current stage. Because of this difficulty, an alternative way to formulate the thermal dispersion is to adopt the thermal dispersion model that has been well-studied in the literature. Based on the suggestions of Xuan and Roetzel (2000) and Khaled and Vafai (2005), the thermal dispersion model developed in the porous media is extended to model the thermal dispersion effect in the nanofluid flow. Based on these suggestions, the thermal dispersion in nanofluid flow is related to the particle volume fraction, fluid thermal capacity, flow domain size, flow velocity and a constant that accounting for effects due to particle size, shape, and random motion, i.e.,

$$k_\mathrm{d} = C^*(\rho C_\mathrm{p})_\mathrm{nf}\phi(H/2)u \tag{16}$$

where C^* is a constant that need to be determined by matching with the experimental data.

Eq. (14) is regarded as the theoretical model for the nanofluid viscosity proposed by Brinkman (1952). For particle volume less than 5%, it has been shown the theoretical and empirical models for nanofluid viscosity agree very well (Ding and Wen, 2005). It should be noted that the nanofluid viscosity could also depend on the particle shape. However, there is no theoretical model available in the literature. As a consequence, the viscosity model shown in Eq. (14) is used in this study.

3. Solution

3.1. Fluid flow and temperature distributions

Using the mean fluid velocity u_m and channel height H as the characteristic velocity and length and define the dimensionless temperature and pressure as

$$\theta_\mathrm{s} = \frac{T_\mathrm{s} - T_\mathrm{w}}{\frac{q_\mathrm{w}H}{(1-\varepsilon)k_\mathrm{s}}}, \quad \theta_\mathrm{f} = \frac{T_\mathrm{f} - T_\mathrm{w}}{\frac{q_\mathrm{w}H}{(1-\varepsilon)k_\mathrm{s}}}, \quad P = \frac{K}{\varepsilon\mu_\mathrm{nf}u_\mathrm{m}}\frac{\mathrm{d}p}{\mathrm{d}x} \tag{16}$$

the governing equations and boundary conditions in dimensionless forms can be written as

$$U = \frac{Da}{\varepsilon}\frac{\mathrm{d}^2U}{\mathrm{d}Y^2} - P \tag{17}$$

$$\frac{\mathrm{d}^2\theta_\mathrm{s}}{\mathrm{d}Y^2} = Bi(\theta_\mathrm{s} - \theta_\mathrm{f}) \tag{18}$$

$$U = Bi(\theta_\mathrm{s} - \theta_\mathrm{f}) + \frac{\varepsilon k_\mathrm{f}}{(1-\varepsilon)k_\mathrm{s}} \times \left[\frac{\partial}{\partial Y}\left(\frac{k_0}{k_\mathrm{f}} + C^*Pe_\mathrm{f}\left(\frac{(\rho c_p)_\mathrm{nf}}{(\rho c_p)_\mathrm{f}}\phi U\right)\frac{\partial\theta_\mathrm{f}}{\partial Y}\right)\right] \tag{19}$$

$$\text{At } Y = 0: \quad U = \theta_\mathrm{s} = \theta_\mathrm{f} = 0 \tag{20a}$$

$$\text{At } Y = 1: \quad U = \frac{\mathrm{d}\theta_\mathrm{s}}{\mathrm{d}Y} = \frac{\mathrm{d}\theta_\mathrm{f}}{\mathrm{d}Y} = 0 \tag{20b}$$

In Eqs. (17)–(19), U is the dimensionless fluid velocity, Da is the Darcy parameter, Y is the dimensionless depth of channel, Bi is the Biot number and Pe_f is the Peclet number. The expressions for these parameters are given as

$$U = \frac{u}{u_\mathrm{m}}, \quad Da = \frac{K}{H^2}, \quad Y = \frac{y}{H}, \quad Bi = haH^2/(1-\varepsilon)k_\mathrm{s}, \quad Pe_\mathrm{f} = \frac{1}{2}(\rho c_p)_\mathrm{f}u_\mathrm{m}H/k_\mathrm{f} \tag{21}$$

The analytical solution of the velocity distribution was solved by Kim and Kim (1999) and given as

$$U = P\left(\cosh\sqrt{\frac{\varepsilon}{Da}}Y + \frac{\left(1-\cosh\sqrt{\frac{\varepsilon}{Da}}\right)}{\sinh\left(\sqrt{\frac{\varepsilon}{Da}}\right)}\sinh\sqrt{\frac{\varepsilon}{Da}}Y - 1\right) \tag{22}$$

Using the condition of $\int_0^1 U\,dY = 1$, the dimensionless pressure can be evaluated as

$$P = \frac{\sinh\sqrt{\frac{\varepsilon}{Da}}}{2\sqrt{\frac{Da}{\varepsilon}}\left[\cosh\sqrt{\frac{\varepsilon}{Da}}-1\right] - \sinh\sqrt{\frac{\varepsilon}{Da}}} \tag{23}$$

In dimensional form, the pressure drop across the MCHS can be evaluated by integrating the pressure gradient along the MCHS length from the definition of dimensionless pressure drop, i.e.,

$$\Delta p = -\frac{12\mu_{nf}u_m P}{W_{ch}^2}L_{hs} \tag{24}$$

Substituting Eq. (22) into Eq. (19) and coupling with Eq. (18), temperature distributions in both the solid and fluid can be solved subject to boundary conditions described in Eq. (20). To avoid tedious mathematical manipulation, temperature distributions in solid and fluid are solved numerically. The derivatives in these equations are replaced by finite difference schemes with second order accuracy.

3.2. Thermal resistance of the MCHS

The MCHS performance is commonly measured by its thermal resistance. By neglecting the thermal resistance at the base plate of MCHS, thermal resistance of MCHS can be written as

$$R_{th} = R_{flow} + R_{fin} \tag{25}$$

where R_{flow} is the convective thermal resistance due to coolant heating as it absorbs energy passing through the channel and R_{fin} represents the conductive thermal resistance due to the heat conduction through the fins and convection from the fins into the coolant. These two quantities can be expressed as

$$R_{flow} = \frac{1}{(\rho c_p)_{nf}\dot{V}}, \quad R_{fin} = \frac{1}{\bar{h}A_{eff}} \tag{26}$$

where $\dot{V}$ is the coolant volume flow rate, $\bar{h}$ is the overall heat transfer coefficient of MCHS, and A_{eff} is the effective heat transfer area. The volume flow rate can be calculated by the expression,

$$\dot{V} = N\rho_{nf}W_{ch}Hu_m \tag{27}$$

where N is the number of channels defined as

$$N = W_{hs}/(W_{ch} + W_{fin}) \tag{28}$$

By neglecting the fin efficiency, the effective heat transfer area can be written as

$$A_{eff} = L_{hs}W_{hs}\varepsilon(1+2\alpha_s) \tag{29}$$

The overall MCHS heat transfer coefficient can be defined as

$$\bar{h} = q_w/(T_w - T_b) \tag{30}$$

where $T_w - T_b$ is the temperature difference between MCHS bottom wall and bulk fluid flow. Using the definition of dimensionless fluid temperature, $T_w - T_b$ can be expressed as

$$T_w - T_b = -\frac{q_w H}{(1-\varepsilon)k_s}\int_0^1 U\theta_f Y\,dY \tag{31}$$

Substituting Eqs. (27), (29) and (31) into Eq. (26), R_{flow} and R_{fin} can be expressed as

$$R_{flow} = -\frac{12\mu_{nf}L_{hs}P}{(\rho c_p)_{nf}W_{ch}^3\alpha_s\Delta p W_{hs}\varepsilon} \tag{32}$$

$$R_{fin} = -\frac{\theta_{fb}H}{\varepsilon(1-\varepsilon)k_s L_{hs}W_{hs}(1+2\alpha_s)} = -\frac{W_{ch}\alpha_s\int_0^1 U\theta_f\,dY}{\varepsilon(1-\varepsilon)k_s L_{hs}W_{hs}(1+2\alpha_s)} \tag{33}$$

For a given MCHS geometry, it is seen from Eq. (32) that using the nanofluid would not reduce the convective thermal resistance since $(\rho c_p)_{nf}$ is usually smaller than $(\rho c_p)_f$ and μ_{nf} is larger than μ_f. The MCHS improvement using a nanofluid relies on a reduction in conductive thermal resistance, as indicated in Eq. (33) which depends on the temperature difference between the bulk nanofluid and MCHS bottom wall. The pumping power required to drive the fluid flowing through the MCHS is defined as

$$\text{Pow} = (\Delta p)\dot{V} \tag{34}$$

4. Results and discussion

4.1. Velocity and temperature distributions in MCHS

In this study, the MCHS made of silicon wafer is considered. Two kinds of nanofluids, copper–water (Cu–H_2O) and carbon nanotube–water (CNT–H_2O) were used as the working fluids. The Cu nanoparticle is assumed to be spherical so that the shape factor SH is equal to 3. The carbon nanotube is assumed to be rod-like with a shape factor of 6 (Gosselin and da Silva, 2004). It is known that carbon has a thermal conductivity of 1200 W/mK, which is about three times larger than that of copper.

In Fig. 2, the velocity distributions in MCHS for two channel aspect ratios are shown for the case of $\varepsilon = 0.5$ and various particle volume fractions based on Eqs. (22) and (23). Note that the case of $\phi = 0$ corresponds to the pure fluid. Since $\varepsilon/Da = 12\alpha_s^2$, the velocity distribution in MCHS depends only on the aspect ratio and fluid viscosity. For $\alpha_s = 2$ case shown in Fig. 2a, velocity has a parabolic profile. Although the particle volume fraction is low, the nanofluid viscosity increases with the increase in particle volume fraction. The presence of nanoparticles has the effect of decreasing the fluid velocity. For $\phi = 2\%$ and

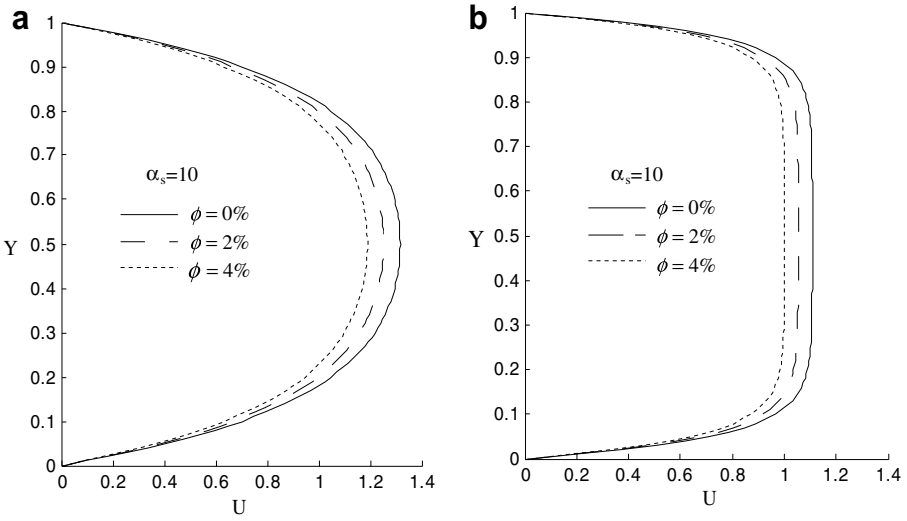

Fig. 2. Dimensionless velocity distributions in MCHS. (a) $\alpha_s = 2$ and (b) $\alpha_s = 10$.

4%, there are about 10% and 20% decreases in velocity magnitudes at the channel centers as compared with that of pure fluid, respectively. For $\alpha_s = 10$ case shown in Fig. 2b, the velocity profiles become flat at the MCHS central region instead of parabolic. Similar to the $\alpha_s = 2$ case, the presence of nanoparticles results in decreasing the velocity magnitude. The velocity profiles shown in Fig. 2 agree well with the theoretical prediction given by Shah and London (1978).

To compute the temperature distribution, the empirical constant C^* appearing in Eq. (16) must be specified. According to the study of Khaled and Vafai (2005) in which heat transfer of nanofluid flow in a channel was investigated, the range of the value of C^* was chosen from 0 to 0.4. Note that the case of $C^* = 0$ corresponds to no thermal dispersion effect. Since the channel flow in the study of Khaled and Vafai (2005) is similar to the microchannel flow in the MCHS and the main purpose of this study is to address the general performance of the MCHS when nanofluid is used as working fluid, the value of $C^* = 0.4$ used in their study is adopted in this study. In Fig. 3, temperature distributions in MCHS for both solid and fluid phases are shown for $\varepsilon = 0.5$, $\alpha_s = 2$ and various particle volume fractions when Cu–H_2O is used. It is seen that the presence of nanoparticle has an effect of raising the fluid temperature. That is, the mean nanofluid temperature is closer to the MCHS bottom wall temperature compared with the pure fluid case. Based on the Newton's cooling law, it implies that the heat transfer coefficient in nanofluid flow is enhanced because of decrease in temperature difference between wall and bulk fluid when constant heat flux is applied at the wall. Referring to Eq. (33), it can also be realized that the conductive thermal resistance can be reduced because of the smaller temperature difference between the MCHS bottom wall and bulk fluid. No significant differences in temperature distributions caused by the nanoparticle presence were found in the solid phase. Temperature profiles of both solid and fluid for the case of $\alpha_s = 10$ are shown in Fig. 4 for the Cu–H_2O cooled MCHS. Similar variation trends in the temperature distributions in both solid and fluid phases are observed except that the degree of temperature raised due to the presence of nanoparticles is not as significant as in the $\alpha_s = 2$ case. Again according to Eq. (33), reduction in conductive thermal resistance would not be significant since the reduction in the temperature difference between the MCHS bottom wall and bulk fluid is not significant. Both temperature profiles of solid and fluid phases for the CNT–H_2O cooled MCHS with $\alpha_s = 2$ and 10 are shown in Figs. 5 and 6, respectively. The temperature variation trends in CNT–H_2O cooled MCHS are the same as those for the Cu–H_2O nanofluid except that a smaller temperature difference is obtained between the MCHS bottom wall and bulk fluid. A larger reduction in conductive thermal resistance in CNT–H_2O cooled MCHS can be expected.

Based on the results shown in Figs. 3–6, it is seen that the solid temperature distributions seem to be independent with the types of the nanofluid used. The same conclusion can also be made from the study of Koo and Kleinstreuer (2005). This conclusion provides an opportunity to verify the correctness of the model presented in this study. In Fig. 7, the solid temperature distributions computed by Koo and Kleinstreuer (2005) at a location of $x = 0.008$ m and by the present model are compared for MCHS with $\varepsilon = 0.5$ and $\alpha_s = 6$ and for pure water and Cu–H_2O nanofluid. It is seen that there is about 4% difference between the temperature distributions shown in Fig. 7. It is suspected that the solid temperature distribution in the study of Koo and Kleinstreuer (2005) is still in the thermally developing region. Since our result is obtained under thermal fully development condition. This reason causes the discrepancy between the results shown in Fig. 7. As indicated in our study and in the study of Koo and Kleinstreuer (2005), nanofluid temperature distribution depends on the

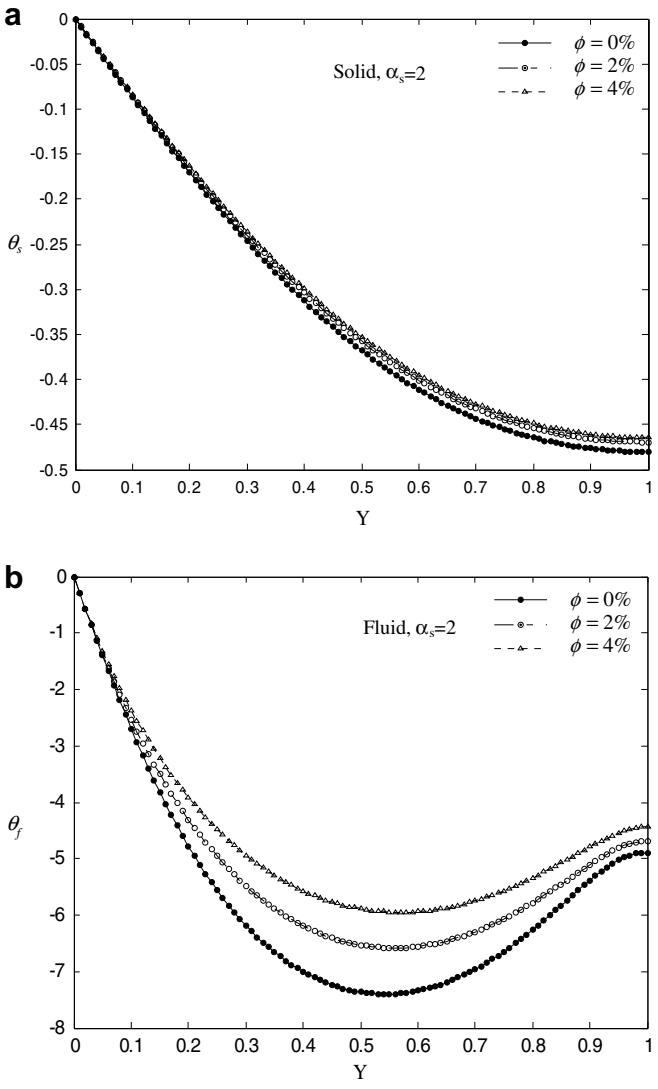

Fig. 3. Dimensionless temperature distributions in MCHS using Cu–H_2O with various particle volume fractions as coolants, $\alpha_s = 2$, $\varepsilon = 0.5$. (a) Solid phase and (b) fluid phase.

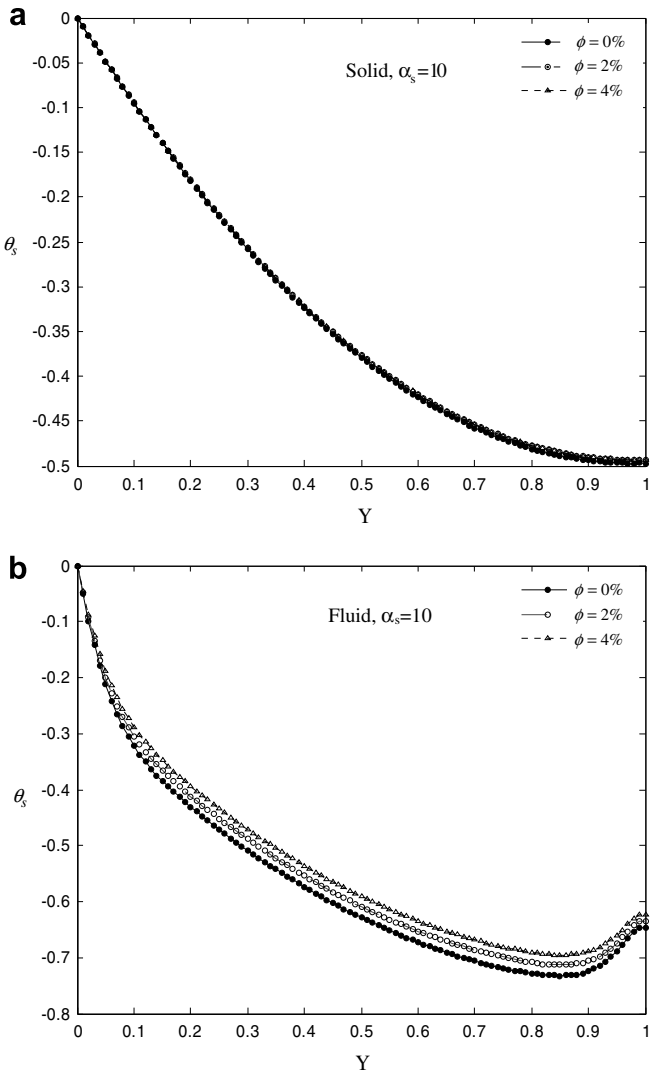

Fig. 4. Dimensionless temperature distributions in MCHS using Cu–H_2O with various particle volume fractions as coolants, $\alpha_s = 10$, $\varepsilon = 0.5$. (a) Solid phase and (b) fluid phase.

type of nanofluid used and boundary conditions. We therefore did not compare our predictions with those of Koo and Kleinstreuer (2005) since different nanofluids and boundary conditions are involved. However, the variation trend of the fluid temperature distribution predicted by our model agrees with that computed by Koo and Kleinstreuer (2005) except at the top side of the microchannel.

4.2. Thermal resistance of nanofluid-cooled MCHS

Eqs. (32) and (33) show that the MCHS thermal resistance are functions of many parameters such as α_s, ε, W_{ch}, ϕ, W_{hs}, L_{hs}, and Δp. To focus on the nanofluid effect, we fixed the MCHS size at $W_{hs} = L_{hs} = 1$ cm and channel depth at $H = 360$ μm. ϕ, α_s and ε are allowed to vary for examining the nanoparticle and channel geometry effects on nanofluid-cooled MCHS performance. In practical MCHS operations, the coolant is supplied to MCHS by an externally connected pump. For a given flow rate and a specified MCHS channel aspect ratio, the mean velocity can be computed from Eq. (27). Consequently, the pressure drop across the MCHS and the required pumping power can be computed from Eqs. (24) and (34), respectively. In Fig. 8, relations between pressure drop and pumping power for CNT–H_2O cooled MCHS with $\varepsilon = 0.5$ are shown. For $\alpha_s = 2$ and 10, the channel widths are 180 μm and 36 μm, respectively. As a result, there are more channels having smaller hydraulic diameter in the MCHS with $\alpha_s = 10$ as compared with the MCHS with $\alpha_s = 2$. Moreover, larger effective heat transfer area can be obtained in the $\alpha_s = 10$ case as compared with $\alpha_s = 2$ case. As shown in Fig. 8, larger pressure drop occurs for $\alpha_s = 10$ case as compared with the $\alpha_s = 2$ case under the same pumping power. This is expected since it is more difficult to drive the coolant into the MCHS when the microchannels are small. Consequently, smaller flow rate can be driven into MCHS when

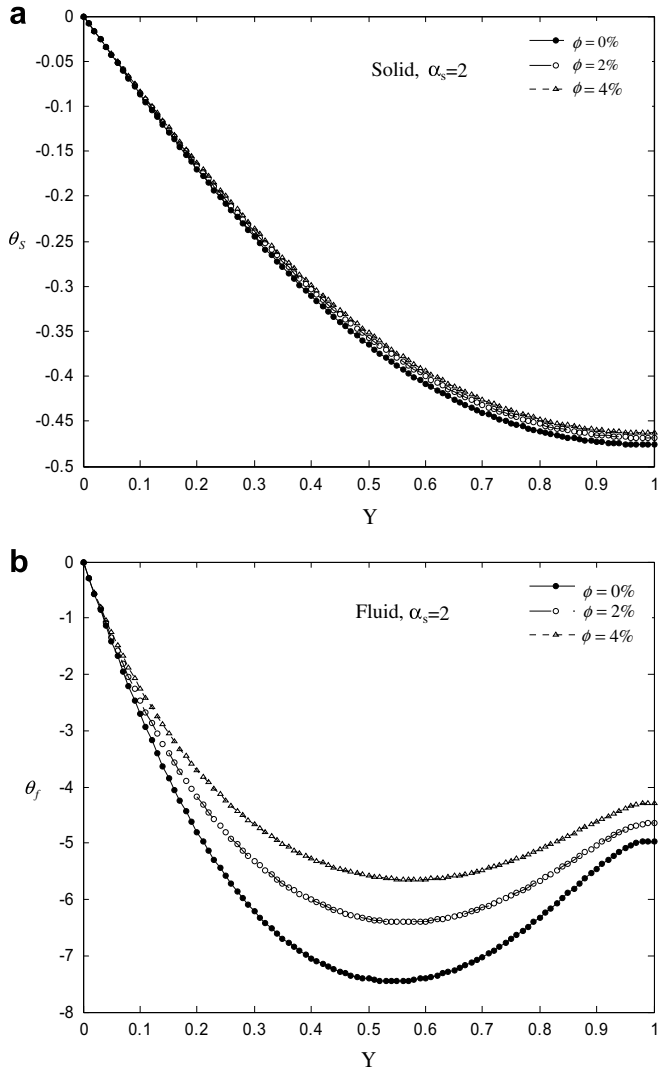

Fig. 5. Dimensionless temperature distributions in MCHS using CNT–H_2O with various particle volume fractions as coolants, $\alpha_s = 2$, $\varepsilon = 0.5$. (a) Solid phase and (b) fluid phase.

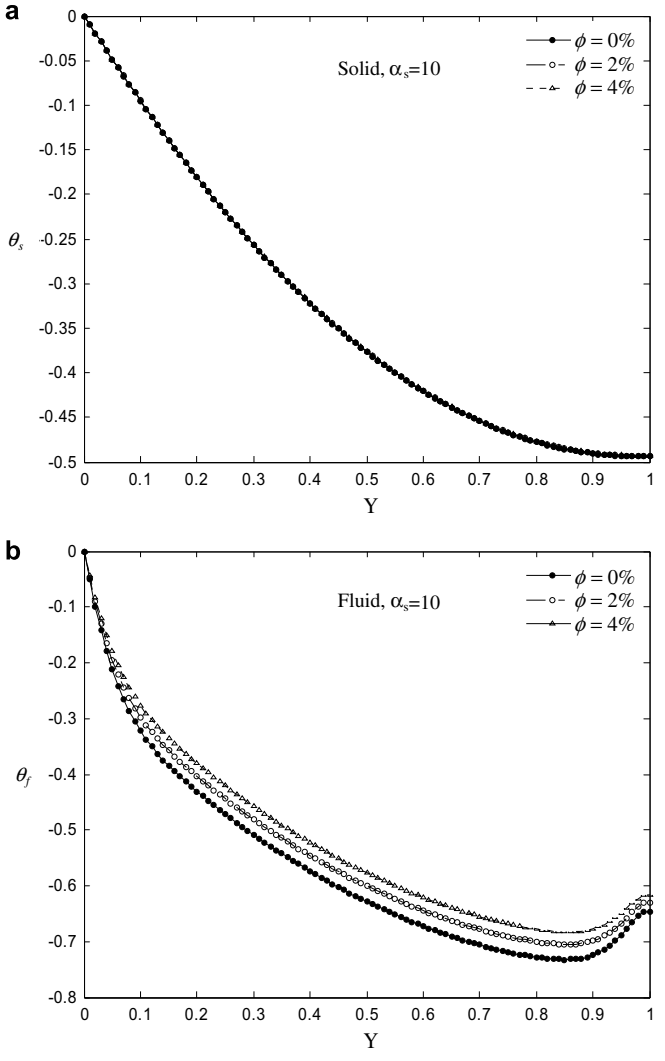

Fig. 6. Dimensionless temperature distributions in MCHS using CNT–H_2O with various particle volume fractions as coolants, $\alpha_s = 10$, $\varepsilon = 0.5$. (a) Solid phase and (b) fluid phase.

α_s is large under the same pumping power. It is also noted that the presence of nanoparticles produces an effect of increasing the pressure drop according to the results shown in Fig. 8. For the case of $\alpha_s = 10$, $\phi = 4\%$, and Pow = 2 W, about 7% increase in pressure drop is found as compared with that of pure fluid.

Recently, Jang and Choi (2006) developed a new model to describe the effective thermal conductivity of nanofluid and used it to investigate the MCHS performance numerically. The nanofluids they used are the Cu–H_2O and diamond–H_2O nanofluids. The particle volume fraction for each nanofluid is 1%. Using these nanofluids and MCHS with $\alpha_s = 8.6$ and $\varepsilon = 0.5$, the predicted thermal resistances as a function of pumping power using the present model are compared with those of Jang and Choi (2006) and shown in Fig. 9. It is seen that the variation trend is in good agreement. For pure water, our predicted thermal resistance is almost identical to that predicted by Jang and Choi

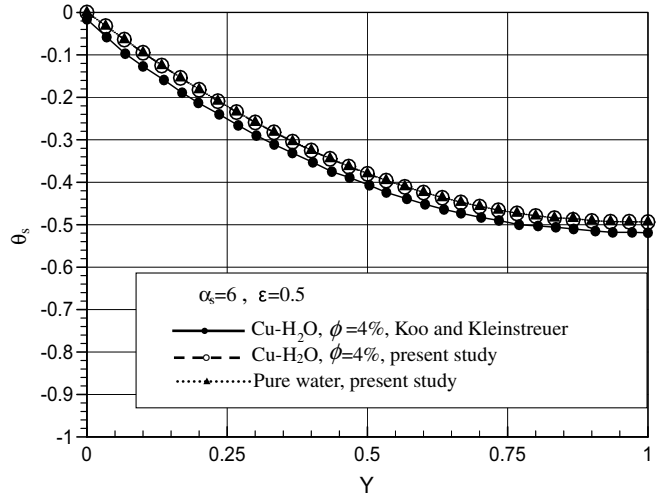

Fig. 7. Comparison of solid temperature distributions predicted by the model proposed in this study and that computed in the study of Koo and Kleinstreuer (2005), $\varepsilon = 0.5$, $\alpha_s = 6$.

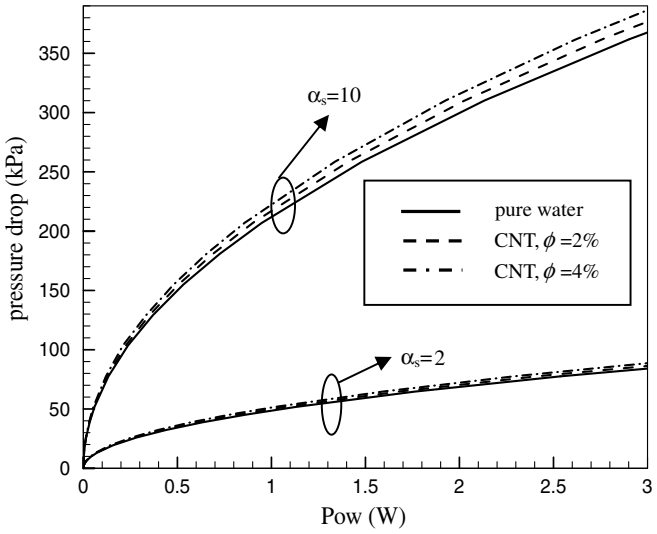

Fig. 8. Pressure drops across pure water cooled- and CNT–H_2O cooled-MCHS as functions of pumping power and channel aspect ratio, $L_{hs} = 1$ cm, $W_{hs} = 1$ cm, $H = 360$ μm, $\varepsilon = 0.5$.

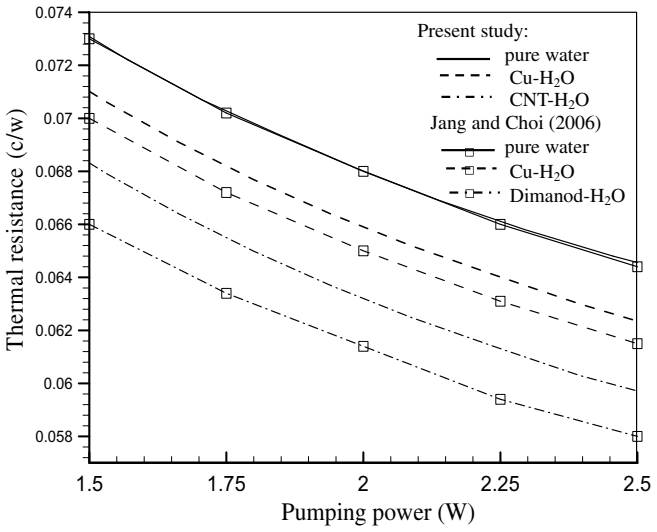

Fig. 9. Comparisons of the thermal resistance predicted using the model proposed in this study with those computed by Jang and Choi (2006), $\varepsilon = 0.5$, $\alpha_s = 8.6$, $\phi = 1\%$.

(2006). Because of the different thermal dispersion models, slightly difference in the value of the thermal resistance is found between our predicted thermal resistance and that of Jang and Choi (2006) when nanofluids are used. Based on the comparisons shown in Figs. 7 and 9, it is believed that the model developed in this study produces satisfactory results and can be extended to further study on the heat sink performance optimization using nanofluid as the working fluid.

In order to have more detail understanding on the effect of nanofluid on the MCHS thermal performance, the convective, conductive and total thermal resistances for nanofluid-cooled MCHS are computed for various channel aspect ratios. In Fig. 10a, the convective, conductive and total thermal resistances for Cu–H_2O cooled MCHS are shown with $\alpha_s = 2$, $\varepsilon = 0.5$, and $\phi = 4\%$. The coolant pumping power is used as a parameter. It is seen that the total thermal resistance is dominated by the conductive thermal resistance since the flow rate is large and effective heat transfer area is small. Compared with pure water cooled MCHS, the convective thermal resistance increases when nanofluid is employed as the coolant. However, the conductive thermal resistance is reduced when using the nanofluid. An improvement in total thermal resistance results because the reduction in conductive thermal resistance is larger compared to the increase in convective thermal resistance. The MCHS performance with $\alpha_s = 10$ using Cu–H_2O under the same operation condition as that in $\alpha_s = 2$ case is shown in Fig. 10b. In contrast to the $\alpha_s = 2$ case, both the convective and conductive thermal resistances are equally important for the MCHS total thermal

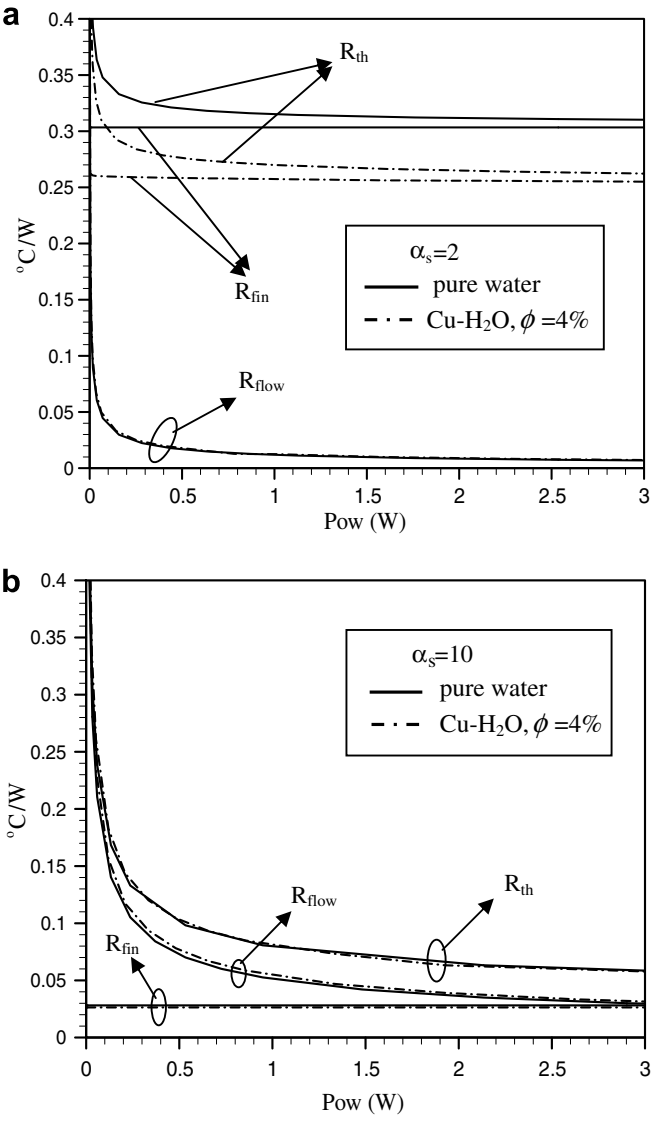

Fig. 10. Thermal resistance of Cu–H_2O cooled MCHS as a function of pumping power, $L_{hs} = 1$ cm, $W_{hs} = 1$ cm, $H = 360$ μm, $\varepsilon = 0.5$. (a) $\alpha_s = 2$ and (b) $\alpha_s = 10$.

resistance. Since the effective heat transfer area is large, much smaller conductive thermal resistance is found as compared with the $\alpha_s = 2$ case. This leads to total thermal resistance of $\alpha_s = 10$ case is much smaller than that of $\alpha_s = 2$ case. It is seen that the presence of nanoparticle has insignificant effect on increasing the convective thermal resistance and decreasing the conductive thermal resistance. The combined effect is that nanofluid has an insignificant effect on MCHS performance enhancement. Using the same conditions for the results shown in Fig. 10, CNT–H_2O cooled MCHS performance is shown in Fig. 11. Since the carbon has higher thermal conductivity as compared with the copper, better MCHS performance is expected when using the CNT–H_2O nanofluid for both channel aspect ratios studied.

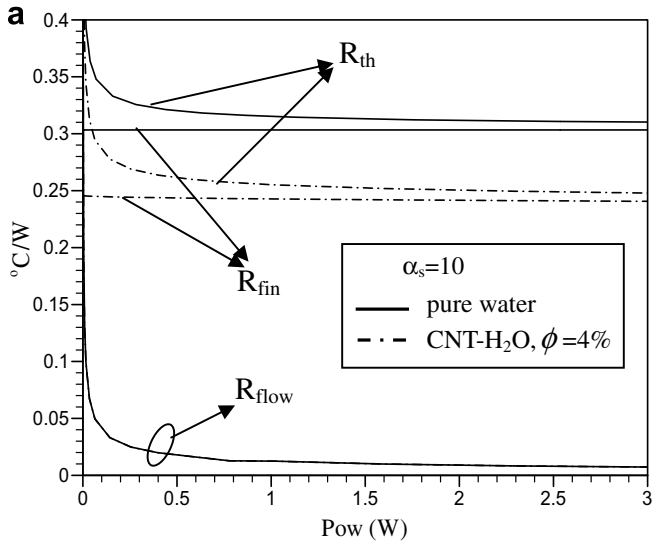

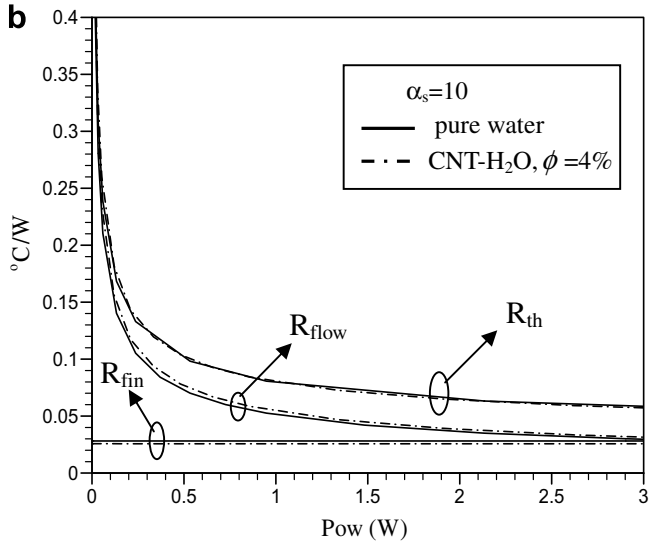

Fig. 11. Thermal resistance of CNT–H_2O cooled MCHS as a function of pumping power. $L_{hs} = 1$ cm, $W_{hs} = 1$ cm, $H = 360$ μm, $\varepsilon = 0.5$. (a) $\alpha_s = 2$ and (b) $\alpha_s = 10$.

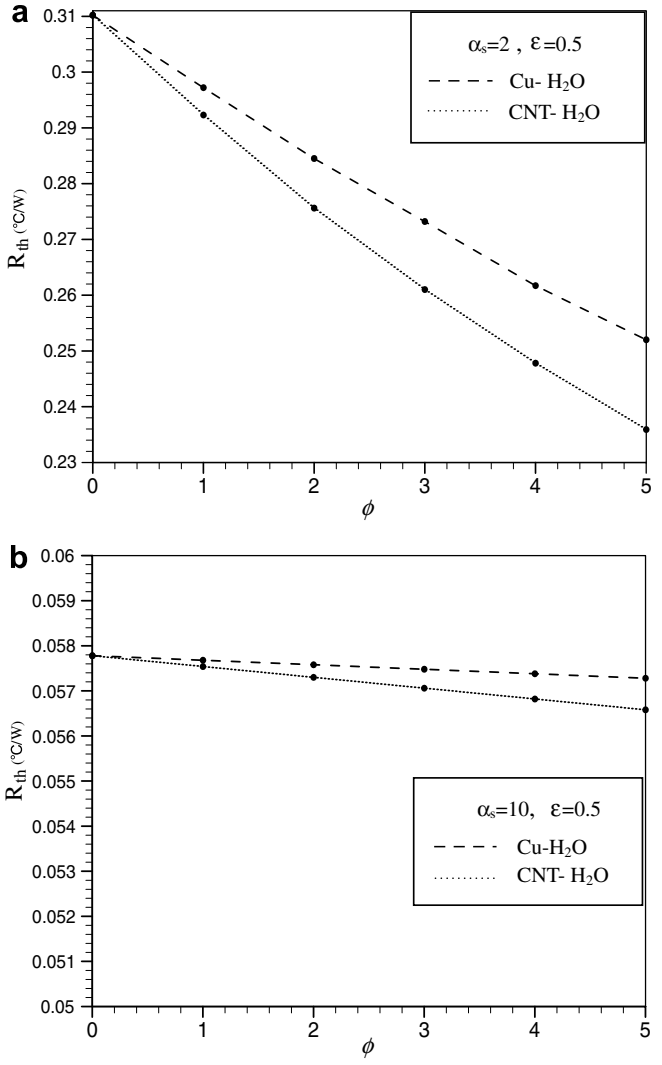

Fig. 12. Thermal resistance of nanofluid-cooled MCHS as a function of particle volume fraction, Pow = 3 W. (a) $\alpha_s = 2$ and (b) $\alpha_s = 10$.

Dependences of MCHS performance on the particle volume fraction are shown in Fig. 12. In Fig. 12, the MCHS geometric configurations are the same as those in Fig. 10 with the coolant pumping power fixed at 3 W. As expected, the thermal resistance of MCHS decreases with the increase in particle volume fraction. More significant thermal resistance reduction is found for $\alpha_s = 2$ case. The effect of nanoparticle on the MCHS thermal resistance becomes insignificant for the $\alpha_s = 10$ case. The reasons for these observations have been described above. For both channel aspect ratios shown in Fig. 12, it is seen that CNT–H_2O cooled MCHS has better performance than the Cu–H_2O cooled MCHS.

Both porosity and the channel aspect ratio are related to the pressure drop across and flow rate through the MCHS. Any variation in these two parameters results in changes in pressure drop and flow rate. It is therefore difficult to compare the MCHS performance under the same pumping power when the channel geometry is varied. Instead of pumping power, effects of porosity and channel aspect

ratio on MCHS performance are examined and compared under a given pressure drop across the MCHS as suggested in the studies of Li et al. (2004) and Li and Peterson (2006). From the definitions, porosity depends on the ratio of channel width to fin width. The limiting values of ε approaching to zero and approaching to unity correspond to very thick and very thin fins in MCHS, respectively. For thin fin case, large number of channel can be resulted and the effective heat transfer area increases. The MCHS has a smaller number of channels and more effective heat transfer area when the fins are thick. In Fig. 13, the MCHS performance as function of ε are shown for $\alpha_s = 2$ and 10. Since pressure drop is proportional to the flow rate, higher pressure drop implies higher flow rate is driven into the MCHS. As shown in Fig. 13a, there is no significant difference between the results between two pressure drops studied when $\alpha_s = 2$. As mentioned above, thermal resistance is dominated by the conductive thermal resistance when aspect ratio is low. The contribution of convective thermal resistance is less important. When the porosity increases, it implies that more channels can be fabricated in MCHS. This results in increasing the heat transfer area and reducing both the conductive and total MCHS thermal resistances. This also implies that MCHS performance can be enhanced using fins with smaller thickness. This finding is agreed with the study of Hunt and Tien (1988) in which they pointed out conduction through porous media is dominant when thick ligaments of porous media was used. However, the fin thickness should be larger enough to withstand the pressurized fluid flow. Also shown in Fig. 13a, use of nanofluid can further decrease the thermal resistance, especially when porosity is low. For $\alpha_s = 10$ case as shown in Fig. 13b, it is found that pressure drop has significant effect on the MCHS thermal resistance. It is noted that convective thermal resistance is inversely proportional to the flow rate. Increasing pressure drop implies that the convective resistance can be reduced. As shown in Fig. 13b, much smaller thermal resistance can be obtained when pressure drop is 200 kPa since the convective thermal resistance is lower. In contrast to the $\alpha_s = 2$ case, using nanofluid does not enhance the MCHS performance, although the difference is not significant. The reason for this observation is clearly due to the combined result between the increased convective thermal resistance and decreased conductive thermal resistance. Also shown in Fig. 13b, an optimum value of ε that producing the lowest thermal resistance can be found for both pressure drops studied.

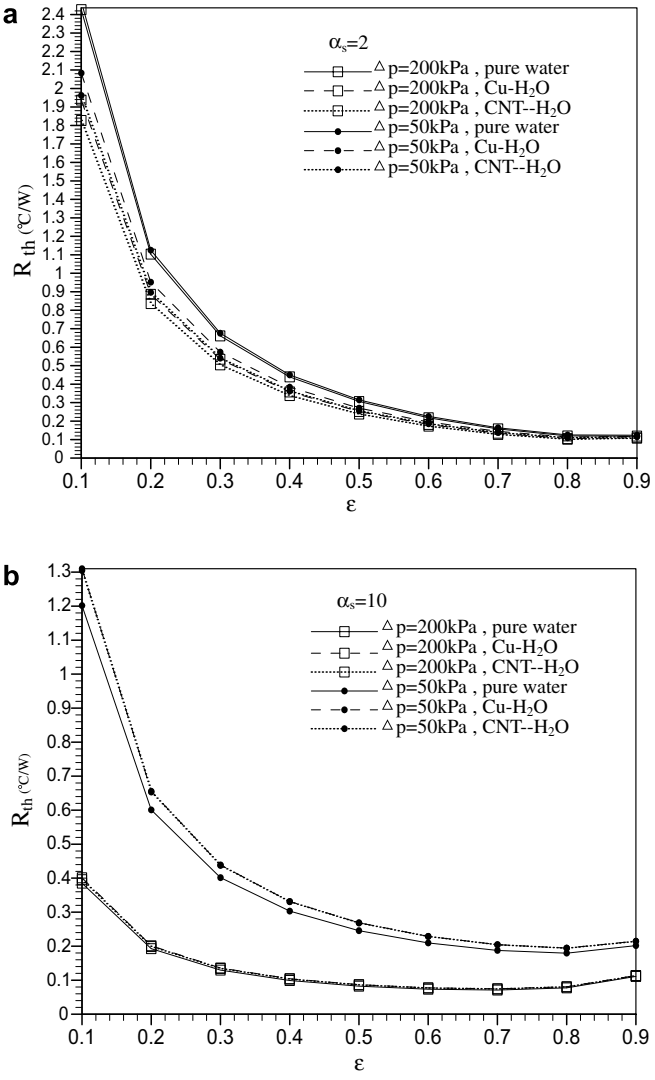

Fig. 13. Total thermal resistance of MCHS as function of ε under condition of constant pressure drop condition, $\phi = 4\%$. (a) $\alpha_s = 2$ and (b) $\alpha_s = 10$.

The effect of channel aspect ratios on the MCHS performance are shown in Fig. 14 for the nanofluid-cooled MCHS with $\varepsilon = 0.5$ and $\phi = 4\%$. For the case of pressure drop equal to 50 kPa, an optimum value of α_s that producing the lowest thermal resistance can be found with a value approximately equal to 5. For α_s less than 5, MCHS performance is enhanced when nanofluid is used. However, when α_s is greater than 5, the nanofluid does not improve MCHS performance. Similar observation can be found when pressure drop increases to 200 kPa as shown in Fig. 14b. For pressure drop equal to 200 kPa, optimum value of α_s is approximately equal to 6. Again, for α_s less than the optimum values for the pressure drops studied, use of nanofluid can enhance the MCHS performance while nanofluid does not affect the MCHS performance very much when α_s are greater than the optimum values. The reasons for this observation are the same as those described in the discussion on the porosity effect on MCHS performance.

4.3. Nanofluid cooled MCHS performance with optimized channel geometry

The results shown in Figs. 13 and 14 indicated that there appears optimum microchannel channel geometry that resulting in the lowest thermal resistance and many investigations have done in the past to address microchannel

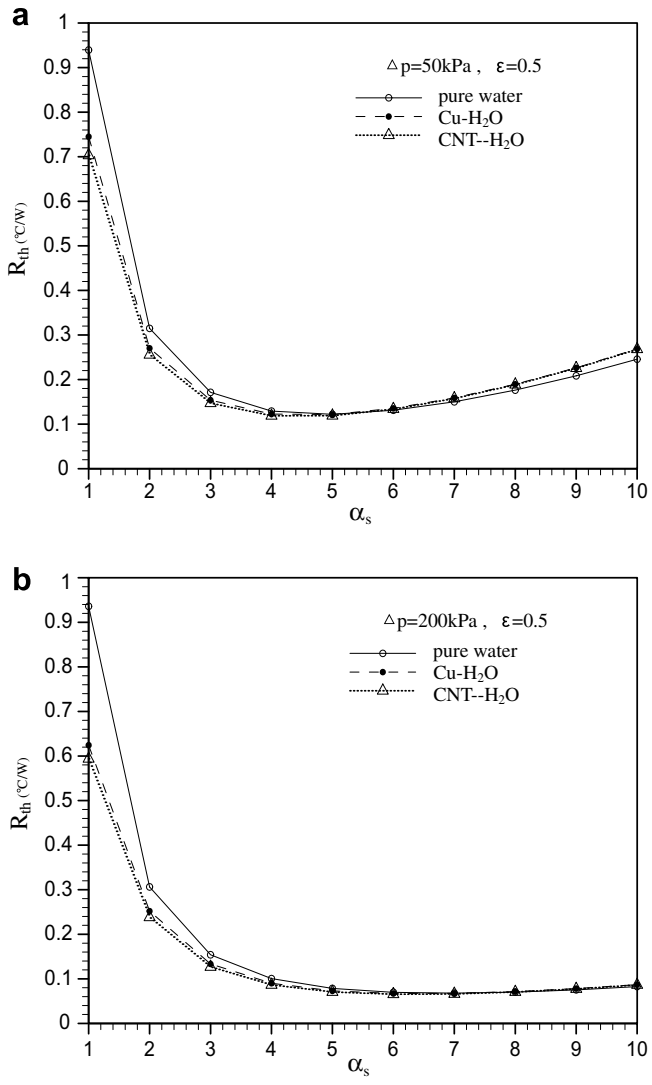

Fig. 14. Total thermal resistance of MCHS as function of channel aspect ratio under condition of constant pressure drop across MCHS, $\phi = 4\%$. (a) 50 kPa and (b) 200 kPa.

geometry optimization (Knight et al., 1992; Li and Peterson, 2006). In this study, we focus on the effect of using nanofluid as coolant in the MCHS and detail of microchannel optimization is not performed. To compare the performances between pure water cooled and nanofluid-cooled MCHS with optimum microchannel geometry, we adopt the results in the study of Tuckerman and Pease (1981). Using the same operation conditions and microchannel geometry in the study of Tuckerman and Pease (1981), the pure water cooled and nanofluid-cooled MCHS performances are summarized in Table 1. It is seen that nanofluid-cooled MCHS can reduce the thermal resistance from 0.086 °C/W to 0.0657 °C/W and 0.0642 °C/W when Cu–H_2O and CNT–H_2O with $\phi = 4\%$ are used as coolants, respectively.

5. Conclusion

In this study, the MCHS performance using nanofluid as coolants is examined. Two kinds of nanofluids, Cu–H_2O and CNT–H_2O are employed in this study. The MCHS structure is modeled as the porous medium and two-equation model are employed to describe the fluid and heat transfer in the MCHS. The obtained flow velocity and temperature distributions are then used to evaluate the thermal resistance that characterizes the MCHS performance. The nanofluid is assumed to be a single-phase fluid. Based on our study, the following conclusions can be made:

(1) The presence of nanoparticles has the effect of reducing the temperature difference between MCHS bottom wall and bulk nanofluid as compared with that of pure fluid. The reduction of this temperature difference is proportional to the particle volume fraction. The degree of reduction in this temperature difference is also found to depend on the channel aspect ratio.
(2) The presence of nanoparticles increases the convective thermal resistance of the MCHS due to the increase in viscosity and decrease in the thermal capacity. The reduction in the temperature difference between MCHS bottom wall and bulk fluid due to the presence of nanoparticles results in a reduction in the MCHS conductive thermal resistance.

Table 1
Comparison of performances of pure fluid cooled- and nanofluid-cooled MCHS with optimized channel geometry

	Tuckerman and Pease (1981)	Present study	
Size $L_{hs} \times W_{hs}$	1 cm × 1 cm	1 cm × 1 cm	
Pumping power (W)	2.27 W	2.27 W	
Coolant	Water	Cu–H_2O $\phi = 4\%$	CNT–H_2O $\phi = 4\%$
Numbers of channels	88	88	88
Channel height, H, μm	365 μm	365 μm	365 μm
Fin thickness, W_{fin}, μm	57 μm	57 μm	57 μm
Channel width, W_{ch}, μm	57 μm	57 μm	57 μm
Porosity, ε	0.5	0.5	0.5
Aspect ratio, α_s	6.4	6.4	6.4
R_{flow}, °C/w	0.022	0.0242	0.0242
R_{fin}, °C/w	0.064	0.0415	0.0400
R_{th}, °C/w	0.086	0.0657	0.0642

(3) The nanofluid has a significant effect on the MCHS performance when the channel aspect ratio and porosity are low. The total thermal resistance can be reduced by the reduction in conductive thermal resistance due to the reduction in temperature difference between mean nanofluid temperature and MCHS bottom wall. For MCHS with high channel aspect ratio and porosity, it is found that using nanofluid does not produce significant MCHS performance enhancement because of large effective heat transfer area.

(4) Under a given pressure drop across the MCHS, optimum values of aspect ratio and porosity that producing the minimum thermal resistance can be found. Using nanofluid can enhance the MCHS performance when the porosity and aspect ratio are less than the optimum porosity and aspect ratio. Using the operation conditions and optimum channel geometry in the study of Tuckerman and Pease (1981), further reduction in MCHS thermal resistance can be resulted when nanofluid is used as the coolant.

References

Ambatipudi, K.K., Rahman, M.M., 2000. Analysis of conjugate heat transfer in microchannel heat sinks. Numerical Heat Transfer Part A 37, 711–731.

Bejan, A., 1984. Convective Heat Transfer. Wiley-Interscience, New York, USA.

Bergles, A.E., 2002. ExHFT for fourth generation heat transfer technology. Experimental Thermal and Fluid Science 26, 335–344.

Brinkman, H.C., 1952. The viscosity of concentrated suspension and solutions. Journal of Chemistry Physics 20 (1952), 571–581.

Chein, R., Chuang, J., 2007. Experimental microchannel heat sink performance studies using nanofluids. International Journal of Thermal Sciences 46, 57–66.

Chein, R., Hunag, G., 2005. Analysis of microchannel heat sink performance using nanofluids. Applied Thermal Engineering 25, 3104–3114.

Crowe, C., Sommerfield, M., Tsuji, Y., 1998. Multiphase Flows with Droplet and Particles. CRC Press, Boca Raton, Florida, USA.

Ding, Y., Wen, D., 2005. Particle migration in a flow of nanoparticle suspension. Powder Technology 149, 84–92.

Ding, Y., Alias, H., Wen, D., Williams, R.A., 2006. Heat transfer of aqueous suspensions of carbon nanotubes (CNT nanofluids). International Journal of Heat and Mass Transfer 49, 240–250.

Fedorov, A.G., Viskanta, R., 2000. Three-dimensional conjugate heat transfer in the microchannel heat sink for electronic packaging. International Journal of Heat and Mass Transfer 43, 399–415.

Gosselin, L., da Silva, A.K., 2004. Combined heat transfer and power dissipation optimization of nanofluid flows. Applied Physics Letters 85, 4160–4162.

Hamilton, R.L., Crosser, O.K., 1962. Thermal conductivity of heterogeneous two-component systems. I and CE Fundamentals 1, 187–191.

Hunt, M.L., Tien, C.L., 1988. Effects of thermal dispersion on forced convection in fibrous media. International Journal of Heat and Mass Transfer 31, 301–310.

Jang, S.P., Choi, S.U.S., 2006. Cooling performance of a microchannel heat sink with nanofluids. Applied Thermal Engineering 26, 2457–2463.

Kandlikar, S.G., Grande, W.J., 2003. Evolution of microchannel flow passages – thermohydraulic performance and fabrication technology. Heat Transfer Engineering 24, 3–17.

Khaled, A.R.A., Vafai, K., 2005. Heat transfer enhancement through control of thermal dispersion effects. International Journal of Heat and Mass Transfer 48, 2172–2185.

Kim, S.J., Kim, D., 1999. Forced convection in microstructures for electronic equipment cooling. ASME Journal of Heat Transfer 121, 639–645.

Kim, S.J., Kim, D., Lee, D.Y., 2000. On the local thermal equilibrium in microchannel heat sinks. International Journal of Heat and Mass Transfer 43, 1735–1748.

Knight, R.W., Hall, D.J., Goodling, J.S., Jaeger, R.C., 1992. Heat sink optimization with application to microchannels. IEEE Transactions on Components, Hybrids, and Manufacturing Technology 15, 832–842.

Koo, J., Kleinstreuer, C., 2004. A new thermal conductivity model for nanofluids. Journal of Nanoparticle Research 6, 577–588.

Koo, J., Kleinstreuer, C., 2005. Laminar nanofluid flow in microheat-sinks. International Journal of Heat and Mass Transfer 48, 2652–2661.

Lee, J., Mudawar, I., 2006. Assessment of the effectiveness of nanofluids for single-phase and two-phase heat transfer in micro-channels. International Journal of Heat and Mass Transfer, doi:10.1016/ijheatmasstransfer.2006.08.001.

Lee, S., Choi, S.U.S., Li, S., Eastman, J.A., 1999. Measuring thermal conductivity of fluids containing oxide nanoparticles. Journal of Heat Transfer 121, 280–289.

Lee, P., Garimella, S.V., Liu, D., 2005. Investigation of heat transfer in rectangular microchannels. International Journal of Heat and Mass Transfer 48, 1688–1704.

Li, J., Peterson, G.P., 2006. Geometric optimization of a micro heat sink with liquid flow. IEEE Transactions on Components and Packaging Technologies 29, 145–154.

Li, Q., Xuan, Y., 2002. Convective heat transfer and flow characteristics of Cu–water nanofluid. Science in China E 45, 408–416.

Li, J., Peterson, G.P., Cheng, P., 2004. Three-dimensional analysis of heat transfer in a micro-heat sink with single phase flow. International Journal of Heat and Mass Transfer 47, 4215–4231.

Maiga, S.B.B., Palm, S.J., Nguyen, C.T., Roy, G., Galanis, N., 2005. Heat transfer enhancement by using nanofluids in forced convection flows. International Journal of Heat Fluid Flow 26, 530–546.

Pak, B.C., Cho, Y.L., 1998. Hydrodynamic and heat transfer study of dispersed fluids with submicron metallic oxide particles. Experimental Heat Transfer 11, 151–170.

Qu, W., Mudawar, I., 2002. Experimental and numerical study of pressure drop and heat transfer in a single-phase microchannel heat sink. International Journal of Heat and Mass Transfer 45, 2549–2565.

Shah, R.K., London, A.L., 1978. Laminar Flow Forced Convection in Ducts. Academic Press, San Diego, CA, USA.

Tiselj, I., Hetsroni, G., Mavko, B., Mosyak, A., Pogrebnyak, E., Segal, Z., 2004. Effect of axial conduction on the heat transfer in microchannels. International Journal of Heat and Mass Transfer 47, 2551–2565.

Tuckerman, D.B., Pease, R.F., 1981. High-performance heat sinking for VLSI. IEEE Electronic Devices Letters EDL 2, 126–129.

Wang, X., Mujumdar, A.S., 2007. Heat transfer characteristics of nanofluids: a review. International Journal of Thermal Sciences 46, 1–19.

Wang, X., Xu, X., Choi, S.U.S., 1999. Thermal conductivity of nanoparticle–fluid mixture. Journal of Thermophysics and Heat Transfer 13, 474–480.

Webb, R.L., 1993. Principles of Enhanced Heat Transfer. John Wiley & Sons, New York.

Xuan, Y., Li, Q., 2003. Investigation on convective heat transfer and flow features of nanofluids. ASME Journal of Heat Transfer 125, 151–155.

Xuan, Y., Roetzel, W., 2000. Conceptions for heat transfer correlation of nanofluids. International Journal of Heat and Mass Transfer 43, 3701–3707.

Yang, Y., Zhang, Z., Grulke, E.A., Anderson, W.B., 2005. Heat transfer properties of nanoparticle influid dispersions (nanofluids) in laminar flow. International Journal of Heat and Mass Transfer 48, 1107–1116.

Zhao, C.Y., Lu, T.J., 2002. Analysis of microchannel heat sinks for electronics cooling. International Journal of Heat and Mass Transfer 45, 4857–4869.